

# Goodput in Wireless Backhaul Networks Using IEEE 802.11: A MAC Irregularity Perspective

Ying Qu and Bryan Ng

Victoria University of Wellington, Wellington 6140, New Zealand

Email: {ying.qu, bryan.ng}@ecs.vuw.ac.nz

**Abstract**—A Wireless Backhaul Network (WBN) carries aggregated data from multiple sources to core networks over wireless links. Increasing data rates and network densification have catapulted the IEEE 802.11 protocol as a strong candidate protocol for WBNs. The low-cost of deployment and maintenance, and self-management functionality are salient features of the IEEE 802.11 protocol for WBNs. Existing disc-graph models and signal-to-interference-and-noise (SINR) goodput models are widely used in sensor networks and mesh networks in simulation tools such as ns-2, ns-3, and Qualnet. However, these models have not been adequately studied in real world WBNs. Our empirical data show that in a typical WBN scenario, an irregular goodput pattern is neither conformant to the SINR nor the disc-graph models. We find that topology and interferer proximity impact the WBN goodput at the MAC layer inconsistently leading to what we call MAC irregularity. We go on to identify the cause of MAC irregularity and quantify its impact on WBN goodput.

**Index Terms**—Networks Network management; Wireless access points, base stations, and infrastructure; Programmable networks

## I. INTRODUCTION

Wireless backhaul networks (WBN) are made up of traffic aggregating nodes such as access points, base stations or routers connected via wireless radio links that carry traffic to a backbone network. WBNs are different from cellular networks, sensor network, mesh networks in terms of deployment, topology and traffic characteristics. WBNs adopt different wireless communication technologies such as point-to-point microwave radio, satellite links, IEEE 802.16 WiMax, and an IEEE 802.11 network Ref. [1].

In contrast to the dedicated channels in microwave, satellite, and WiMax, the IEEE 802.11 WBN uses a broadcast channel and therefore brings about a set of unique challenges. Increasing data volumes over the network are driving network operators, service providers and new found uses such as user provided networks Ref. [2] to IEEE 802.11 WBN for lower cost, rapid deployment and efficient solutions.

However, lacking proper empirical data, research in WBNs heavily relied on disc-graph models, SINR models

and stochastic geometry for years. These models characterise the goodput and fairness in terms of physical characteristics such as signal attenuation, propagation models etc. Such models naturally provide a predictable, monotonic goodput variation with distance. However, these models do not account for medium access control (MAC) protocol semantics.

In our research, we first collect empirical data on goodput and fairness from a test WBN. The data suggest that the fit of SINR and disc-graph models to empirical data is poor. At times the analytical/simulation models return false positives (i.e. satisfies goodput and fairness are predicted but not observed in empirical data) and at times the analytical/simulation models yield a false negative (i.e. poor goodput and unfairness are not predicted but observed in empirical data).

Second, we adjusted the empirical data with consideration of signal anisotropy, random effects of the physical channel, capture effect, exposed/hidden terminal and radio irregularities. The adjusted data shows that the MAC layer experiences non-monotonic goodput variations with distance giving rise to statistically significant discrepancies with existing disc-graph and SINR models. Also, this variation is observed under both ideal carrier sensing and non-ideal carrier sensing conditions (detailed in Section II). We define this non-monotonic variation (measured at the MAC layer) in goodput with distance “MAC irregularity” and this is attributed to the complex interaction of the IEEE 802.11 MAC protocol and the node placement in a WBN.

The contribution of this paper is the characterisation of IEEE 802.11 MAC irregularity and verifying its presence through comparing simulation, analysis and empirical data. Findings from our research are of strong relevance to WBNs because it gives insights into network goodput, potential bottlenecks and provides guidelines for WBN deployment that will help avoid low goodput and flow starvation.

We select two simple scenarios, two-link and three-link topologies for the work in this paper because they are the building blocks for larger WBNs. The rest of this paper is organised as follows: Section II summarises the related work and motivates the need for experimental study of MAC irregularity followed by a brief description of analytical models used to predict goodput in Section III. Section IV describes the simulation evaluation, and Section V presents the experiment results followed by the

---

Manuscript received January 14, 2018; revised May 15, 2018.  
Corresponding author email: bryan.ng@ecs.vuw.ac.nz.  
doi:10.12720/jcm.13.6.266-274

conclusion in Section VI. We are requesting that you follow these guidelines as closely as possible.

## II. RELATED WORK

Disc-graph models and signal-to-interference-and-noise (SINR) models are extensively used in simulation tools such as ns-2, ns-3, and Qualnet. These models assume that the MAC layer in IEEE 802.11 WBNs detects the CCA in a consistent and regular fashion and thus, the achieved goodput is fixed for a given transmission power and receiver sensitivity Ref. [3], [4], [5], and [6]. With these models, the goodput pattern is modelled as a binary function of increasing distance. The carrier sensing mechanism between two nodes is “ON” if two nodes are within each other’s carrier sensing range. The carrier sensing mechanism is “OFF” when two nodes are out of carrier sensing range.

When all nodes are either within carrier sensing range or out of carrier sensing range we have what is called an ideal carrier sensing scenario. In ideal carrier sensing, all nodes can hear each other clearly within carrier sensing range and share channel capacity equally Ref. [7], [8], and [9]. Any two links that are out of carrier sensing range may utilise channel capacity available to each node without any contention. When several nodes are within carrier sensing range and several other nodes out of carrier sensing range, the exposed node/hidden nodes problem arises (we refer to this scenario as non-ideal carrier sensing).

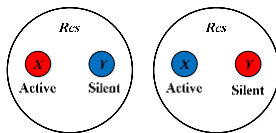


Fig. 1. Carrier sensing mechanism is ON.

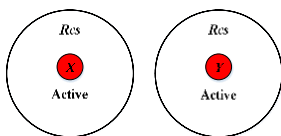


Fig. 2. Carrier sensing mechanism is OFF.

To further illustrate the ideal carrier sensing scenario, we use an example. Consider a simple backhaul network with two nodes (X and Y) and carrier sensing range of two nodes is a disc (with fixed radius) around nodes X and Y. In Fig. 1, Nodes X and Y are within carrier sensing range ( $R_{CS}$ ), thus they cannot transmit concurrently and only either node X or Y can be active. Thus, nodes X and Y share the channel capacity equitably with each receiving its fair share of goodput. The carrier sensing mechanism between nodes X and Y is “ON” in this case. When nodes X and Y are out of carrier sensing range (see Fig. 2), both of them can be active and transmit packets concurrently thus the carrier sensing mechanism between nodes X and Y is “OFF”.

In non-ideal carrier sensing scenarios, serious fairness problems and goodput starvation have been shown to

occur due to border effect Ref. [10]-[13], leading to loss of connectivity in a WBN. The border effect appears in a WBN once the distance between two border links exceeds the carrier sensing range. When border effect happens, border links dominate transmission opportunities and the links situated between the border links achieve very low goodput. In this case, the carrier sensing mechanism between two border links is “OFF” and they are more likely to transmit more packets because these two border links have fewer conflicting links than the links between them (middle links). The middle links are within the carrier sensing range of two border links. Hence, the carrier sensing mechanism between border links and middle links are “ON” and these middle links sense the channel state as busy more frequently than two border links. Consequently, two border links occupy the channel capacity and the links between them get starved.

Several papers have shown that serious fairness problems such as goodput starvation occur in WBNs, and this unfairness is shown to occur in mesh networks and sensor networks Ref. [14], [12], [15]-[17]. Durvy *et al.* Ref. [16] found that border effect causes serious unfairness in IEEE 802.11 wireless networks through mathematical analysis and simulation. WBNs are particularly susceptible to border effect due to the node placement in regular geometric layouts such as a line or a grid. The goodput starvation was also demonstrated through simulations in Ref. [14], [10], [15], [12], and [18], thus reinforcing the findings of analytical models.

Though extensive modelling and simulation studies have been conducted to characterise the goodput of the IEEE 802.11 protocol, there have been little work to reconcile these modelling efforts with empirical data. It is well known that the attenuation of physical signal is a somewhat smooth function of distance and therefore we expect the corresponding variation of goodput should be smooth as the distance between nodes increase. Some researchers argue that existing analytical models make incorrect assumptions about fixed carrier sensing range and binary effect of carrier sensing mechanisms and have called for such models to be validated through experimental work Ref. [19]-[22].

The lack of experimental validation of goodput models for WBNs motivates the work presented in this paper. Specifically, we analyse the goodput pattern from simulation and analytical models against test-bed measurement and provide evidence that the discrepancy between empirical data and analytical/simulation models is attributed to MAC irregularity. The outcome from this study is useful for designing more realistic models to reflect the effect of carrier sensing on goodput.

## III. MAC GOODPUT: ANALYTICAL MODELS

In this section, we analyse the goodput of wireless links in a typical WBN with analytical models of the 802.11 CSMA goodput. We use the analytical model to evaluate the goodput patterns in the two-link and three-

link topologies (corresponding to ideal and non-ideal carrier sensing scenarios). In the analysis, nodes continuously transmit packets to reflect the saturated traffic assumption and packet losses due to collision are ignored. The carrier sensing range is identical and fixed for all nodes. We will compare our analysis with simulation and experimental results in the following sections.

A. Goodput Pattern in Ideal Carrier Sensing: A Two-Link Scenario

Two widely used models for goodput in ideal CSMA scenarios networks are disc-graph model and the signal-to-interference-and-noise (SINR) model Ref. [23]. Both models consider the pairwise interference between two arbitrary nodes and the interference is determined by the distance between the two nodes. The disc-graph model and SINR model are defined in Def. 1 and 3. The definitions in this section use the concept of a conflict set to compute the number of links that will share the network capacity (denoted by C).

**Definition 1: Disc-graph model**  $\gamma_A$

Let  $E$  denote the complete set of links in a WBN. For a tagged link  $i$  in  $E$ , the carrier sensing conflict set,

$$\gamma_A(i) = \{l \in E \setminus \{i\} \mid d_{l,i} \leq R_{cs}, \quad (1)$$

whereby  $d_{l,i}$  is the distance between link  $l$  and link  $i$ ,  $R_{cs}$  is the carrier sensing range. The capacity for each link is:

$$C_A = \frac{c}{\sum_{all\ i} |\gamma_A(i)| + 1}, \quad (2)$$

whereby  $|\gamma_A(i)|$  denotes the cardinality of the set  $\gamma_A(i)$ .

**Definition 2: SINR model**  $\gamma_B$

Let  $E$  denote the complete set of links in a WBN. For a tagged link  $i$  in  $E$ , the carrier sensing conflict set,

$$\gamma_B(i) = \{l \in E \setminus \{i\} \mid P_l + P_{noise} > CS_t\}, \quad (3)$$

whereby  $P_l$  is the signal strength received in link  $i$  from link  $l$ ,  $P_{noise}$  is the signal strength received in link  $i$  from background noise,  $CS_t$  is the carrier sensing threshold. The capacity for each link is:

$$C_B = \frac{c}{\sum_{all\ i} |\gamma_B(i)| + 1}, \quad (4)$$

whereby  $|\gamma_B(i)|$  denotes the cardinality of the set  $\gamma_B(i)$ .

If we ignore the background noise, Def. 3 can be further simplified as:

$$\gamma_B(i) = \left\{ l \in E \setminus \{i\} \mid \left( \frac{1}{d_{l,i}} \right)^\beta > CS_t \right\}, \quad (5)$$

whereby  $\beta$  is the path loss exponent factor,  $CS_t$  is the carrier sensing threshold. This is because  $CS_t$  is a configuration parameter (which is constant), the carrier sensing mechanism is captured in SINR models purely by the distance between two links. Next, we will analyse the goodput patterns in two-link and three-link scenarios.

Using the Def. 1 and 2 above, we analyse the goodput pattern in a two-link WBN. The two-link scenario is the

simplest realisation of a WBN. This two-link WBN shown in Fig. 3 includes two pairs of nodes denoted by  $(S1, R1)$  and  $(S2, R2)$  that are connected through wireless links  $L1$  and  $L2$  respectively. The sender-receiver separation of each pair of nodes and the interferer proximity between links are denoted by  $D_{tr}$  and  $d_{L1,2}$  respectively.

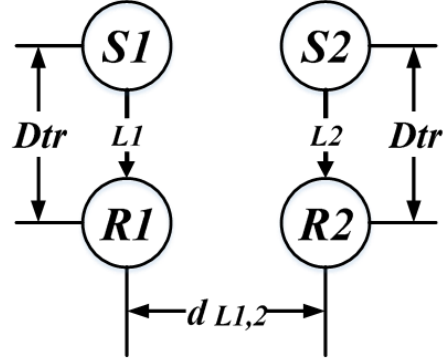


Fig. 3. The two-link scenario

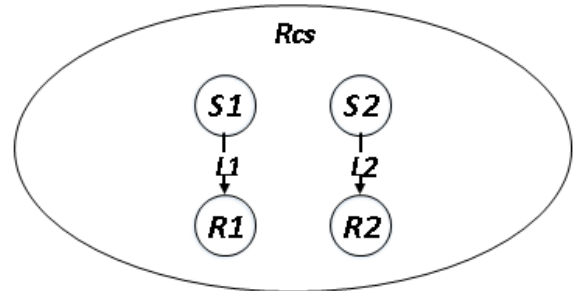


Fig. 4. All four nodes are within each other's carrier sensing range

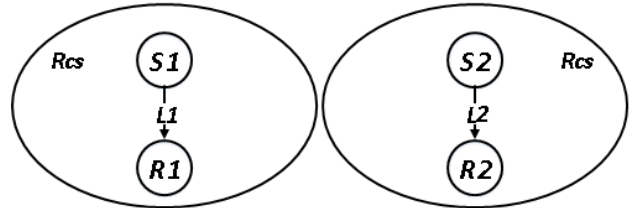


Fig. 5. Two links (sender receiver pair) are beyond each other's carrier sensing range

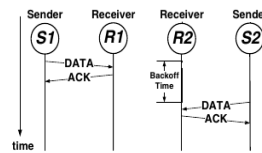


Fig. 6. Time-line diagram for message exchanges between sender and receivers when all four nodes are within each other's carrier sensing range.

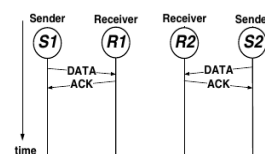


Fig. 7. Time-line diagram for message exchange between sender and receiver when two links are beyond each other's carrier sensing range.

The carrier sensing range is denoted by  $R_{cs}$ . By increasing the link separation distance  $d_{L12}$  (shown in Fig. 3), the links  $L1$  and  $L2$  will be either within or out of each other's carrier sensing range ( $R_{cs}$ ), and this is defined as "State 1" and "State 2" respectively.

**Definition 3: State 1: all nodes are within each other's carrier sensing range.** — In this state, links  $L1$  and  $L2$  remain within  $R_{cs}$  (see Fig. 4), which means no two nodes can transmit simultaneously.

As an example, consider the nodes shown in Fig. 4, using the disc-graph model to compute the goodput distribution in a WBN, we have  $\gamma_A(L1) = L2$  and likewise  $\gamma_A(L2) = L1$ . Invoking (2) to calculate the average goodput of a link, we have  $C_A = \frac{C}{2}$ , which suggests that the goodput of each link is shared equally between  $L1$  and  $L2$ . This can be reasoned using the time-line diagram of message exchange between sender and receiver in links  $L1$  and  $L2$  using the CSMA/CA semantics shown in Fig. 6. In State 1, links  $L1$  and  $L2$  share the channel capacity equally and collisions do not occur in this state. In Fig. 6 and 7, DATA denotes a unicast data packet and ACK denotes an acknowledgment packet.

**Definition 4: State 2: Links  $L1$  and  $L2$  are out of one each other's carrier sensing range.** — We increase the distance  $d_{L12}$  such that it is greater than  $R_{cs}$  (as shown in Fig. 5), which means the carrier sensing mechanism does not reduce the goodput between links  $L1$  and  $L2$ .

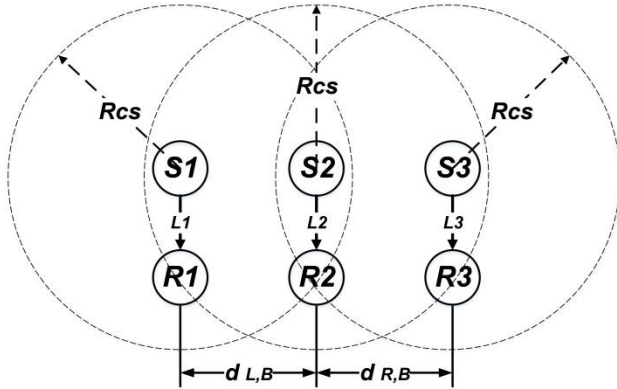


Fig. 8. A Three-link scenario

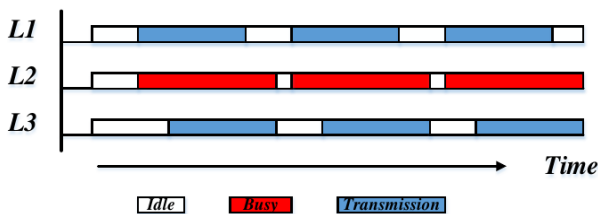


Fig. 9. Transmissions on  $L1$ ,  $L2$  and  $L3$  as a function of time in the three-link scenario

Again, we use an example to illustrate links in State 2. Consider the nodes shown in Fig. 5, using the disc-graph model to compute the goodput distribution in the WBN, we have  $\gamma_A(L1) = \emptyset$ , similarly  $\gamma_A(L2) = \emptyset$ . Invoking (2) to calculate the average goodput of a link, we have  $C_A = C$ , and this is true for both  $L1$  and  $L2$ . Both links achieve

goodput of the link capacity and this is explained with the time-line diagram in this state is shown in Fig. 7. Links  $L1$  and  $L2$  occupy the channel capacity independently and there are no interference and no collisions between them.

### B. Goodput Pattern in Non-ideal Carrier Sensing: A Three-Link Scenario

To study the goodput pattern under non-ideal carrier sensing conditions, we add a third link to the two-link scenario. In Fig. 8, the links  $L1$  and  $L3$  are the two border links that are beyond each other's carrier sensing range while link  $L2$  is in the middle and within the carrier sensing range of both links  $L1$  and  $L3$ .

**Definition 5: Independent set:** Let  $E$  denote the complete set of links in a WBN. For a tagged link  $i$  in a network  $E$ , the independent set,

$$IS(i) = \{l \in E \setminus \{i\} \mid d_{l,i} > R_{cs}\} \quad (6)$$

whereby  $d_{l,i}$  is the distance between link  $l$  and link  $i$ ,  $R_{cs}$  is the carrier sensing range.

**Definition 6: Conflict set:** The conflict set of a tagged link  $i$ ,

$$\gamma(i) = \{l \in E \setminus \{i\} \mid d_{l,i} \leq R_{cs}\} \quad (7)$$

whereby  $d_{l,i}$  is the distance between link  $l$  and link  $i$ ,  $R_{cs}$  is the carrier sensing range and it is clear that  $IS(i) \cup \gamma(i) \cup i = E$ .

**Definition 7: Goodput:** The goodput of a tagged link  $i$  is defined as the ratio between goodput and maximum net bandwidth.

$$G(i) = \begin{cases} 0, & d_{L,B} \leq R_{cs} \wedge d_{R,B} \leq R_{cs} \\ \frac{\chi(i)}{\chi(i) + \sum_{j \in \gamma(i)} \chi(j)}, & \text{otherwise} \end{cases} \quad (8)$$

whereby  $R_{cs}$  is the carrier sensing range,  $d_{L,B}$  is the distance between a link and the left border link,  $d_{R,B}$  is the distance between a link and the right border link, and  $\chi(i)$  denotes the number of links in a given  $IS(i)$ .

Based on our model Ref. [24], in Fig. 8, link  $L2$ 's conflict set is  $\{L1, L3\}$  and the conflict set of  $L1$  and  $L3$  are  $\{L2\}$ . Link  $L2$ 's independent set is  $\emptyset$  so the goodput of  $L2$  is predicted as "0". The independent set of  $L1$  and  $L3$  are  $\{L3\}$  and  $\{L1\}$  respectively. Therefore, these two border links are predicted to achieve the whole capacity as "1" according to (8).

This result can also be explained by Fig.9, the transmissions that occur on  $L1$  and  $L3$  are dependent on the state of  $L2$  however the transmission of  $L2$  is dependent of both the state of  $L1$  and  $L3$ . Therefore, based on CSMA semantics,  $L2$  is more likely to be starved as  $L1$  and  $L3$  will continue occupying the channel.

### C. A Regular Goodput Pattern Emerges

From the predictions of analytical models presented in sections III–A and B, we summarise our evaluations as follows:

- 1) Based on the definitions of analytical models, the carrier sensing range is fixed for a given transmission power and receiver sensitivity.

- 2) The carrier sensing mechanism in both the disc-graph models and SINR models is a binary function of the distance between two links. Within the carrier sensing range, the carrier sensing mechanism between two nodes is “ON” while the carrier sensing mechanism between them is “OFF” when two nodes are out of carrier sensing range.

#### IV. SIMULATION PREDICTIONS FOR GOODPUT

In this section, we evaluate the goodput performance of the two-link and three-link scenarios described earlier in Section III through simulations with Qualnet 5.2. Qualnet 5.2 utilises the disc-graph and signal-to-interference-and-noise (SINR) models for IEEE 802.11 CSMA Ref. [25].

All nodes are configured with identical parameters shown in Table I. The reason for choosing IEEE 802.11b is to simplify the system model without the added physical layer complexity such as multiple-input and multiple-output technology. To ensure collision-free transmissions, the sender-receiver distance  $D_{tr}$  is set to 50–200m based on the finding that CSMA protects against collision when the  $D_{tr}$  of a link is less than  $0.56 \times D_{tr}^{Max}$  (where  $D_{tr}^{Max}$  denotes the maximum transmission range) Ref. [25].

TABLE I: SIMULATION CONFIGURATION PARAMETERS

Parameter Name	Value
Transmission Power	15dBm
Receiver Sensitivity	-83dBm
Path Loss Model	Two-Ray
Shadowing and Fading Model	None
Antenna type	Omni-directional
Routing	Static Routing
Physical Layer	IEEE 802.11b
Data Rate	11Mbps
Traffic Generation	Constant Bit Rate
Packet Size	1500Bytes
Inter-packet Interval	0.5ms

The theoretical maximum transmission range  $D_{tr}^{Max}$  in this simulation is calculated by QualNet’s radio range utility with the simulation configuration (topology) as input. The value of  $R_{cs}$  is calculated based on three factors:

- (i) the minimum receiver sensitivity of  $-94$  dBm,
- (ii) maximum transmission power of 15dBm (based on Linksys WRT1900ac), and
- (iii) the two-ray wireless propagation model.

All results shown in this section are averages from 100 randomly seeded simulation runs. The averages shown are reported with confidence interval of 95% with the range from 0.72 to 2.0kbps under the assumption that the averages are normally distributed.

##### A. A Goodput Pattern Emerges

In this subsection, we evaluate the goodput pattern in two-link (see Fig. 3) and three-link (see Fig. 8) WBNs as

the distance between links are increased. In Fig. 10, the goodput of links  $L1$  and  $L2$ , are evaluated at different distances by increasing  $d_{L1,2}$ . The distance  $d_{L1,2}$  is varied from 50m to 800m with 50m increments. Links  $L1$  and  $L2$  transit from State 1 to State 2 (defined in Def. 3 and 4) at distance  $d_{L1,2} = 700$ m. It matches the theoretical carrier sensing range, calculated as  $R_{cs} = 700$ m Ref. [12].

1) Goodput pattern in a two-link scenario: For goodput variation, the step-function curve for goodput shown in Fig. 10 matches the expected behavior of wireless links predicted by the analytical models in Section III. When interferer proximity is smaller than  $R_{cs} = 700$ m, links  $L1$  and  $L2$  are aware of one another’s transmission effectively coalescing both links into a single link with two senders. It is clear that senders in both links are in State 1 and the capacity is shared equally (3.14 Mbps each).

As the interferer proximity increases greater than  $R_{cs}$  (i.e. the links transition to State 2), the communicating links effectively behave as two independent networks thus explaining the higher goodput (6.29Mbps). The links  $L1$  and  $L2$  are in State 2 and transmissions on each link achieves full capacity (as given by Def. 4). Again, we see that the simulation results agree with the predictions from the analytical models.

2) Goodput pattern in a three-link scenario: In the three-link scenario, two border links  $L1$  and  $L3$  are separated with border distance of 800m while  $L2$  is positioned in the middle between them. All nodes are static during the simulation.

Again, the results from simulation (see Fig. 11) match the analytical predictions given by Def. 4. Both links  $L1$  and  $L3$  achieve the maximum goodput. It shows that when two border links are out of the each others’ carrier sensing range, the carrier sensing mechanism is not active between them and hence no reduced goodput due to carrier sensing mechanism is observed. The middle link  $L2$  is starved due to the border effect.

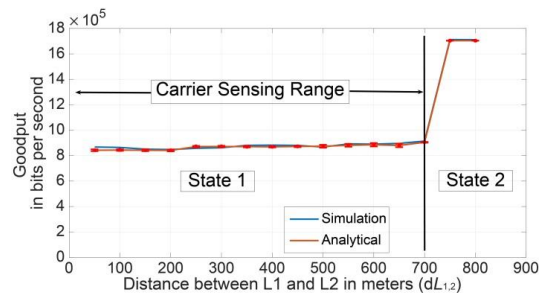


Fig. 10. Goodput in the two-link scenario  $D_{tr} = 50$ m

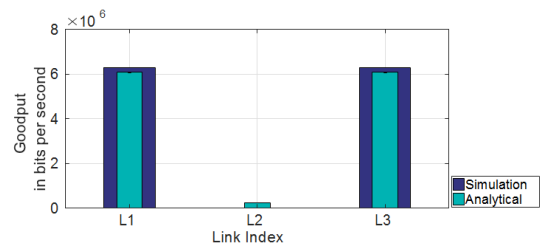


Fig. 11. Goodput in the three-link scenario  $D_{tr} = 50$ m

**B. Simulation Results Agree with Predictions from Analytical Models**

Overall, the simulation results match the predictions from analytical models. These results suggest that the goodput in a WBN exhibits a regular pattern with clear delineation (akin to a binary function) of goodput as a function of distance. Moreover, in non-ideal carrier sensing scenarios, serious fairness problems such as goodput starvation are expected to occur.

**V. EMPIRICAL RESULTS FOR GOODPUT**

In this section, we validate the analytical model and simulation results through experimental measurement.

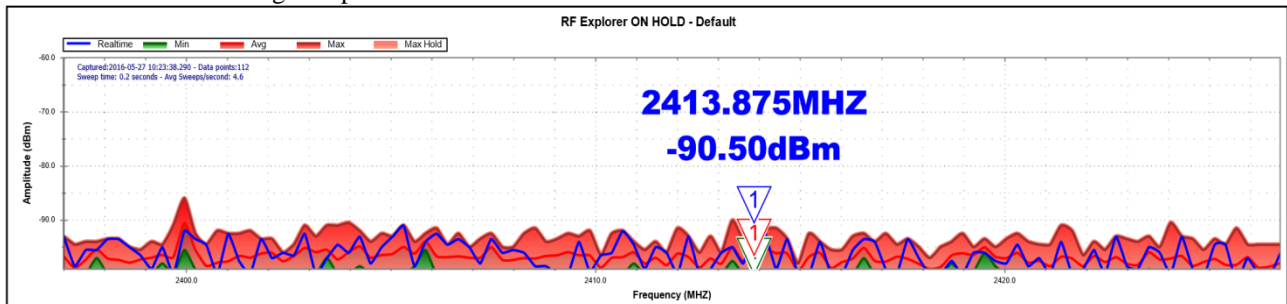


Fig. 12. Background spectrum analysis in the experiment field

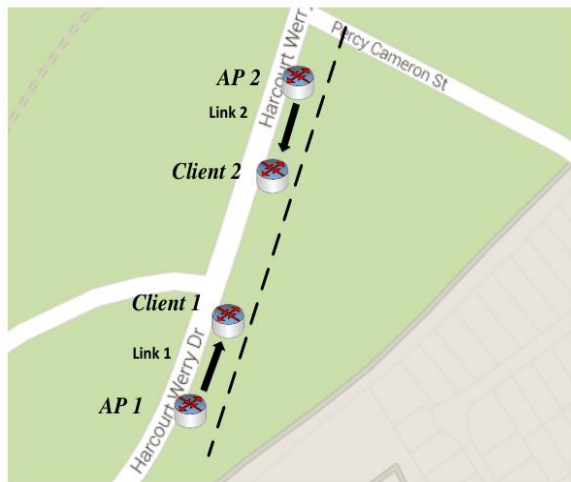


Fig. 13. Outdoor scenario with two links in a line topology

The spectrum analyser passively scans the frequency span from 2397MHz–2427MHz; the minimum, maximum and average power (in dBm) are recorded and plotted as linearly interpolated lines in Fig. 12. It is clear that there is minimal WiFi pollution in Channel 1 with a maximum background power recorded as -90.50dBm.

All APs in the experiment are of the same model (Linksys WRT1900ac) and using OpenWrt 15.05 on Linux. Each AP is operating in the 2.412 GHz band (Channel 1) using the IEEE 802.11b protocol and has four Omni-directional antennas with a maximum data rate of 11 Mbps (at the physical layer).

The measurements were conducted between April and July 2016. All results shown in this section are averages from 10 samples. The averages shown are reported with confidence interval of 95% with the range from 24 to 68

Firstly, we describe the outdoor test environment and hardware configuration, then examine the experimental results and finally compare with simulation and analysis results obtained earlier in Sections III and IV.

**A. Test-bed Environment**

To further validate the analytical models and simulation results, we implemented test-bed experiments in the outdoor environment. The scenarios (Fig. 13, 14 and 15) are the outdoor settings in Lower Hutt, Wellington, New Zealand. Fig. 12 shows the spectrum sweep for the outdoor test location where the tests were conducted.

kbps under the assumption that the averages are normally distributed.

**B. Carrier Sensing Range & Goodput Variation**

For the two-link scenario, we configured the routers with different transmission powers, 4 dBm and 7dBm. Compared with the default transmission power (15 dBm), these reduced transmission powers are used to narrow the transmission range and carrier sensing range for meaningful comparison with our empirical data.

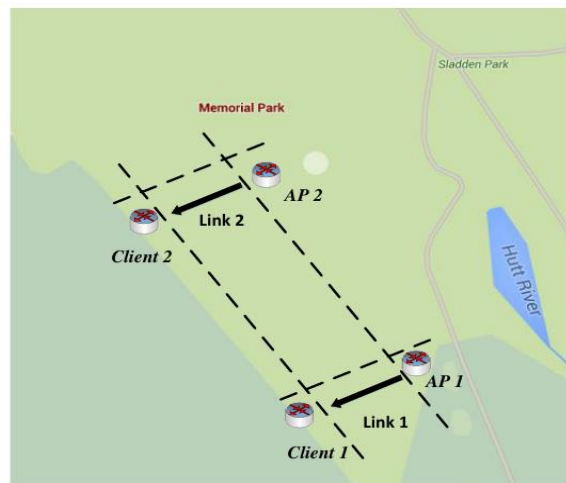


Fig. 14. Outdoor scenario with two links in a grid topology

We use two-link topology in Fig. 14 to validate the ideal carrier sensing scenario with 4 dBm and 7 dBm transmission power. We note that the gradual increment of goodput in Fig. 16 (see topology) is different from the step-like curve in simulation and analytical models (see Fig. 10). The goodput recorded in Fig. 18 shows the same

trend as Fig. 16. The larger distance  $d_{L1,2}$  between two links, the higher the goodput they achieve. In this figure, we cannot determine a fixed carrier sensing range because there is no clear transition point from State 1 to State 2 defined in Section III.

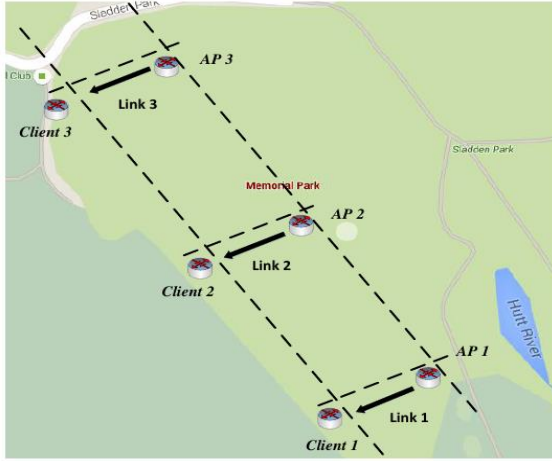


Fig. 15. Outdoor Scenario with three links in a grid topology

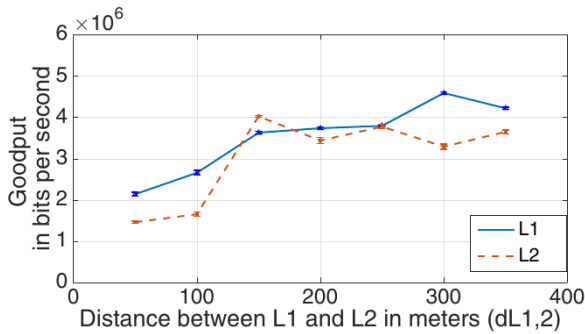


Fig. 16. Two-link experiment in 350x50m2 with 4 dBm power

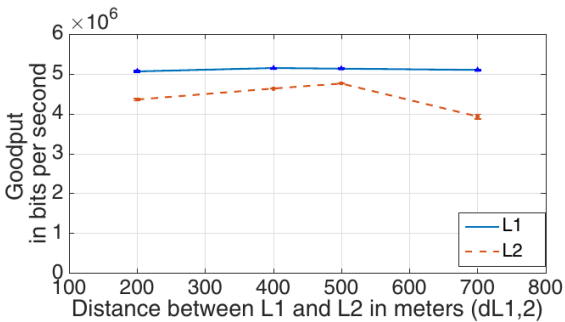


Fig. 17. Two-link experiment in 800m line topology with 7 dBm power

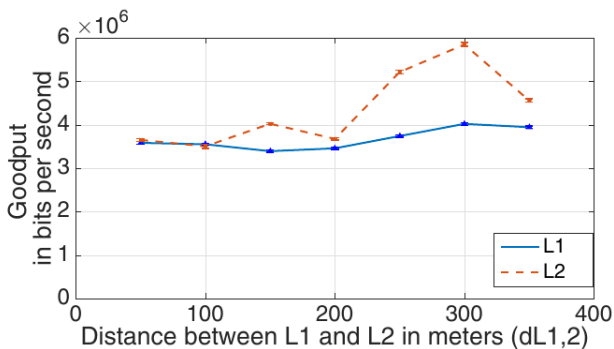


Fig. 18. Two-link experiment in 350x50m2 with 7 dBm power

We use the line topology scenario in Fig. 13 to validate the ideal carrier sensing condition. Fig. 17 shows the goodput pattern from a line topology as the distance between links  $L1$  and  $L2$  increases from 200m to 700m. Both links  $L1$  and  $L2$  achieve the nearly equal goodput because they are within each others' carrier sensing range. The measured goodput agrees with the simulation results shown in Fig. 10 and there is no evidence of MAC irregularity.

For further validation, we evaluate the three-link scenario in Fig. 15 with the routers set to transmit at 4dBm transmission power so that the carrier sensing mechanism is always active between links  $L1$  and  $L3$ . In the experiment, the two border links  $L1$  and  $L3$  remain static and we move the middle link  $L2$  in the range between links  $L1$  and  $L3$ . All three links are under the ideal carrier sensing condition as all three links are within each other's carrier sensing range.

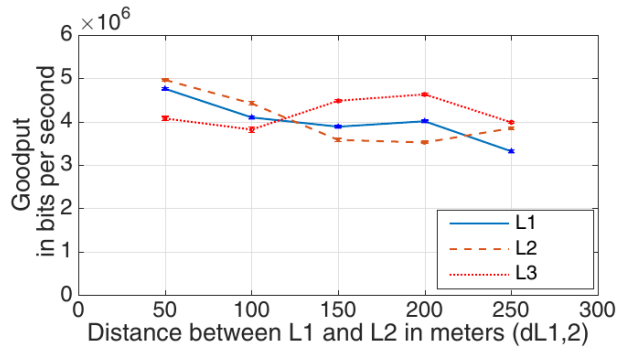


Fig. 19. Two-link experiment in 350x50m2 with 4 dBm power

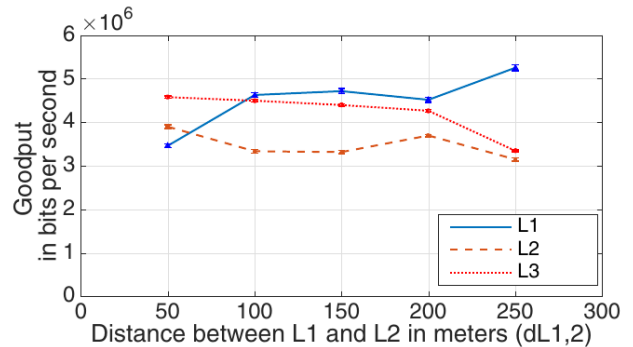


Fig. 20. Two-link experiment in 350x50m2 with 0 dBm power

In Fig. 19, the horizontal axis denotes the distance between middle link  $L2$  and one border link  $L1$ . The result shows that the achieved goodput of links  $L1$ ,  $L2$ , and  $L3$  are nearly equal because carrier sensing mechanism is actively covering all three links.

### C. Border Effect & Starvation

To investigate border effect and starvation predicted by simulation and analytical models, we configured the routers with 0 dBm to narrow the transmission range and carrier sensing range. We keep the distance between two border links  $L1$  and  $L3$  as 350m that is the maximum distance in our experiment field. For Fig. 20, the horizontal axis denotes the distance between middle link

$L2$  and one border link  $L1$ . In Fig. 20, two border links are nearly out of the theoretical  $R_{cs}$  as they are configured with 0 dBm.

The result shows that overall middle link  $L2$  achieves lower goodput than links  $L1$  and  $L3$ , but does not starve (we were expecting to see a graph similar to Fig. 11). When the distance between the middle link  $L2$  and a border link,  $L1$  or  $L3$ , is less than 100m, the goodput of this border link reduces to the same level as that of the middle link.

The discrepancy between the measured goodput and the simulation is attributed to MAC irregularity. In the presence of MAC irregularity, the CCA is inconsistent (flipping between ON and OFF) giving  $L2$  more opportunities for transmissions and therefore preventing it from goodput starvation.

#### D. Discussion

In our experiments under ideal carrier sensing condition, wireless links share the channel capacity nearly equally when the links are close to each other. When two links move further apart, the goodput gradually varies.

The experiment results in the non-ideal carrier sensing scenarios show that unfairness problem exists but the serious goodput starvation does not happen. When the middle link is close to one border link, the middle link and this border link achieve identical goodput as they can sense each other clearly and have to share the channel capacity. Under such circumstances, the other border link achieves higher goodput because it cannot sense the other two links clearly and it senses more opportunities to transmit packets. When the middle link moves towards the middle point between two border links, the goodput of this middle link reduces and two border links achieve higher goodput because the middle link experiences interference from two border links.

The results in test-bed experiments do not match the expectations of analytical model and simulation. These results imply that in real-world scenario, the carrier sensing mechanism is not a binary function of: (i) transmitter receiver separation and (ii) interferer proximity. This observation can be explained by the MAC irregularity in real-world scenarios.

## VI. CONCLUSIONS

In this paper, we study the goodput pattern from existing analytical models for IEEE 802.11 CSMA compared with results from commercial simulation tool and test-bed experiment. The results from experiments show a different trend against the analytical models and simulation results.

We found that the carrier sensing mechanism varies gradually with the (i) distance between communicating nodes and (ii) presence of interferers. Moreover, in non-ideal carrier sensing scenarios, the unfairness among links exists a WBN but we have not observed goodput

starvation and trace this discrepancy due to MAC irregularity. The finding of MAC irregularity can help us refine the existing models to better reflect real world goodput characteristics in simulation tools.

## REFERENCES

- [1] IEEE STD 802.11-1999. Wireless LAN Medium Access Control (MAC) and Physical Layer (PHY) specification, 1999.
- [2] Iosifidis, George and Gao, Lin and Huang, Jianwei and Tassiulas, "Leandros Incentive mechanisms for user-provided networks," *IEEE Communications Magazine*, vol.52, no. 9, pp. 20–27, 2014.
- [3] L. Fu, S. C. Liew, and J. Huang, "Effective carrier sensing in CSMA networks under cumulative interference," *IEEE Transactions on Mobile Computing*, vol. 12, no. 4, pp. 748–760, April 2013.
- [4] C. Thorpe and L. Murphy, "A survey of adaptive carrier sensing mechanisms for IEEE 802.11 wireless networks," *IEEE Communications Surveys Tutorials*, vol. 16, no. 3, pp. 1266–1293, Third 2014.
- [5] Z. Zeng, Y. Yang, and J. C. Hou, "How physical carrier sense affects system throughput in IEEE 802.11 wireless networks," in *Proc. IEEE Conference on Computer Communications*, Phoenix, AZ, USA, April 2008.
- [6] H. Zhai, Y. Fang, *et al.* "Physical carrier sensing and spatial reuse in multirate and multihop wireless ad hoc networks," in *Proc. International Conference on Computer Communications*, Barcelona, Spain, April 2006, pp. 1–12.
- [7] G. Bianchi, "Performance analysis of the IEEE 802.11 distributed coordination function," *IEEE Journal on Selected Areas in Communications*, vol. 18, no. 3, pp. 535–547, 2000.
- [8] G. Bianchi and I. Tinnirello, "Remarks on IEEE 802.11 DCF performance analysis," *IEEE Communications Letters*, vol. 9, no. 8, pp. 765–767, 2005.
- [9] J. S. Reigadas, A. Martinez-Fernandez, J. Ramos-Lopez, and J. Seoane-Pascual, "Modeling and optimizing IEEE 802.11 DCF for long-distance links," *IEEE Transactions on Mobile Computing*, vol. 9, no. 6, pp. 881–896, 2010.
- [10] M. Durvy, O. Dousse, and P. Thiran, "Border effects, fairness, and phase transition in large wireless networks," in *Proc. Conference on Computer Communications*, Phoenix, AZ, USA, April 2008.
- [11] M. Garetto, T. Salonidis, and E. W. Knightly, "Modeling per-flow throughput and capturing starvation in CSMA multi-hop wireless networks," *IEEE/ACM Transactions on Networking*, vol. 16, no. 4, pp. 864–877, 2008.
- [12] C. H. Kai and S. C. Liew, "Temporal starvation in CSMA wireless networks," in *Proc. IEEE International Conference on Communications*, Kyoto, Japan, June 2011, pp. 1–6.
- [13] X. Wang and K. Kar, "Throughput modelling and fairness issues in CSMA/CA based ad-hoc networks," in *Proc. IEEE Conference on Computer Communications* Miami, USA, March 2005, pp. 23–34.
- [14] D. N. M. Dang, P. L. Vo, C. K. Hwang, and C. S. Hong, "Mitigating starvation in wireless ad hoc networks: Multi-

- channel MAC and power control,” in *Proc. ACM International Conference on Ubiquitous Information Management and Communication*, Siem Reap, Cambodia, January 2014, p. 16.
- [15] V. Kolar, S. Razak, and N. B. Abu-Ghazaleh, “Interaction engineering: Achieving perfect CSMA handshakes in wireless networks,” *IEEE Transactions on Mobile Computing*, vol. 13, no. 11, pp. 2552–2565, 2014.
- [16] M. Ghanbarinejad, G. Calcev, and M. Diana, “WiFi-Based mmWave Backhaul-Part 1: Feasibility,” in *Proc. IEEE Globecom Workshops (GC Workshops)*, 2016, pp. 1–6.
- [17] Y. Wang, J. Zhang, J. M. Wang, and B. Bensaou, “Coordinated fair resource sharing in dense indoor wireless network,” in *Proc. IFIP Networking Conference*, 2014, pp. 1–9.
- [18] M. W. Lee, G. Hwang, and S. Roy, “Performance modeling and analysis of IEEE 802.11 wireless networks with hidden nodes,” in *Proc. ACM International Conference on Modeling, Analysis & Simulation of Wireless and Mobile Systems*, Barcelona, Spain, November 2013, pp. 135–142.
- [19] A. Iyer, C. Rosenberg, and A. Karnik, “What is the right model for wireless channel interference?” *IEEE Transactions on Wireless Communications*, vol. 8, no. 5, pp. 2662–2671, 2009.
- [20] S. W. Ng and T. H. Szymanski, “Interference measurements in an 802.11 n wireless mesh network testbed,” in *Proc. IEEE Canadian Conference on Electrical & Computer Engineering*, Montreal, Quebec, April 2012, pp. 1–6.
- [21] V. Sevani and B. Raman, “SIR based interference modeling for wireless mesh networks: A detailed measurement study,” in *Proc. Fourth International Conference on Communication Systems and Networks*, Bangalore, India, January 2012, pp. 1–10.
- [22] G. Zhou, T. He, S. Krishnamurthy, and J. Stankovic, “A impact of radio irregularity on wireless sensor networks,” in *Proc. 2nd ACM Conference on Mobile Systems, Applications, and Services*, 2004, pp. 125–138.
- [23] O. Goussevskaia, Y. A. Oswald, R. Wattenhofer, “Complexity in geometric SINR,” in *Proc. 8th ACM International Symposium on Mobile Ad Hoc Networking and Computing*, 2007, pp. 100–109.
- [24] Y. Qu, B. Ng, and W. K. G. Seah, “A goodput distribution model for IEEE 802.11 wireless mesh networks,” in *Proc. International Performance Computing and Communications Conference*, Nanjing, China, December 2015, pp. 1–8.
- [25] Scalable Network Technologies QualNet 5.2 Programmer’s Guide October, 2011.
- [26] K. Xu, M. Gerla, and S. Bae, “How effective is the IEEE 802.11 RTS/CTS handshake in ad hoc networks,” in *Proc. Global Communications Conference*, Taiwan, November 2002, pp. 72–76.



**Ying Qu** has been working towards the Ph.D. degree in the area of communication and networking at Victoria University of Wellington, New Zealand since 2013. Her main research interests are performance modeling and channel assignment in wireless mesh networks and wireless backhaul networks.



**Bryan Ng** completed his PhD (2010) in the area of communication and networking. He held teaching & research positions in Malaysia and France in addition to attachments to commercial research laboratories Intel, Motorola, Panasonic and Orange Labs. His research interest include performance analysis of communication networks, modelling networking protocols and software defined networking.